Al-Qadisiyah Journal of Pure Science

ISSN(Printed): 1997-2490 ISSN(Online): 2411-3514

DOI: 10.29350/jops

Al-Qadisiyah Journal of Pure Science

Exohedral metallofullerene: Theoretical Insight to Investigate structural, Electronic and Optical Properties Based Complex Single-Molecule.

Shaymaa Khalid Neamah[1] and Qusiy H. Al-Galiby[2]

Department of Physics, College of Education, University of Al-Qadisiyah, Al Diwaniyah 58002, Iraq.

*Corresponding Author: qusiy.algaliby@qu.edu.iq

Received: 19/02/2026; Accepted: 16/03/2026.

Abstract

Exohedral-fullerene has drawn much interest in studying metal complexes of organic molecules. In this work, we used Density Functional Theory (B3LYP-DFT) to investigate the structural, electronic and optical properties of exohedral-metallofullerene. We confirm that these properties can be tuned by varying the transition metal over the set of Co, Cu, Fe, Ni, Pt, and Ru atoms, bounded on the top of external surface of fullerene cage in three central positions: Diatomic π-bond, hexagon and pentagon. The Frontier molecular orbital distribution reveals that the doped C_{60} fullerene by these metals can predict the electronic properties, including ionization potential, electronic affinity, energy gap, electronegativity, hardness, softness, density of states and dipole moment, referring greater potential for molecular interaction. To characterize the optical performance of molecules in the context of time-dependent of DFT, we looked at their absorption spectra in the UV and IR. We found that the six metal atoms are able to tune the optical properties of the complex molecules, providing an insight into sensitivity of doping in the fullerene cage. In the most cases, the favorite positions of the metal atoms can be found on the pentagon and hexagon of the outer surface of the C_{60}. These calculations show that exohedral metallo-fullerenes introduce a new family of electronic and optoelectronic materials with attractive features, which makes those of all metallo-fullerenes for molecular electronic devices and their functionalization.

Keywords: Exohedral-fullerene; complexes organic molecules; density functional theory; electronic optoelectronic materials.

Introduction

Fullerenes have attracted a great interest on account of their potential of the variety functional forms as building blocks for molecular devices, including their high chemical stability, their high electron affinity and their ability to form metallofullerenes by coordinating a metallic atom with enhanced optical, electrical and thermal functionalities [1-6]. A typical carbon cluster of C_{60} fullerene, consisting of 60 carbon atoms (20 hexagons and 12 pentagons) arranged in a spherical cage. The single and double bonds characteristic between the carbon atoms (C-C and C=C), exhibiting strong bond to atom/or molecule. Therefore, in C_{60} fullerene, located an atom or a molecule inside (endohedral) or outside (exohedral) surface of fullerene, leading to a strategic effect of various uses in organic transistors [7], sensors [8], solar cells [9, 10] and thermoelectric devices [11-13].

The earliest experimental study on doping of fullerene C_{60} has been achieved, when iodine was mixed with C_{60} [14]. The later research has explored doping of coevaporated fullerene with an alkali metal yields a radical cluster [15] and the fullerene was doped by nitrogen, which led to reduce the band gap of C_{60} and alters its optical and electronic properties, promising for future sodium-ion batteries applications (SIBs) [16]. Form the point of view of enhancing the efficient electrocatalysts formed from fullerene C_{60} via transition metal-doped, it was found that the metals reveal superior catalytic activity, which introduce a new class of doped fullerene molecules and their applications as effective electrocatalysts for water splitting [17].

As molecular solids, exohedral metallofullerene complexes, when the positively charged metal is coordinated on the external surface of the fullerene cage, have received attention [18-23]. However, more systematic work is still needed to understand the activity of these metals on the outer surface of fullerenes. The different contributions of singly bonded metal in each complex mainly depend on the amount of charge transferred from the metal to fullerene, leading to significantly alter and influence the properties of C_{60} fullerene complexes [24, 25]. Moreover, varying the metal outside the cage of C_{60} can make the chemical reactivity, which opens up for various fields, such as hydrogen storage, catalysis and spin electronic devices [26-28].

In this paper, we present a systematic study of C_{60} fullerenes in interaction with Co, Cu, Fe, Ni, Pt and Ru atoms. We shall investigate the effect of three different bond positions of varied metals on the external surface of C_{60} fullerene, consisting the diatomic-π bond, hexagon and pentagon positions

with new structural, electronic and optoelectronic properties. We predict that in view of this binding, the stable structure can be identified by exploring the favorite position of the metal atoms on the outer surface of the C_{60} and the optoelectronic properties can be tuned with the transition metal complex.

2. Computational Method

As shown in Figures (1-3), the fullerene C_{60} of interest consists three different outer bonds of atomic metal, including the diatomic-π bond (C-C), hexagon (6C-ring) and pentagon (5C-ring) positions. Our aim is to investigate the effect on electronic and optoelectronic performance of varying the metal atom **M** = Co, Cu, Fe, Ni, Pt and Ru metallic atoms.

To calculate the electrical properties of each metallofullerene (M-C60), we used the density functional theory (**DFT**) Gaussian-16 package [29], which employs **B3LYP** to represent hybrid functional with **LanL2DZ** basis set for metallic atom **M** and split valence Pople type basis set **6-31G(d,p)** for carbon atoms. All fullerene C_{60} structures with metallic atoms **M** were optimised with reliable functionals in the ground state.

The (DFT-B3LYP) will use to compute the electronic properties, including the charge transfer, ionization potential (IP), and electronic affinity (EA), energy gap, electronegativity (χ), hardness (η), stuffiness (S) and dipole moment for all metallo-molecules. To understand the optical performance, we use full time-dependent (TD)-DFT for studying the change in the absorption of ultraviolet (UV) and infrared (IR) spectra in response to the binding of metallic atoms.

The electronic properties of C_{60} fullerene with varied metallic atoms such as IP and EA parameters are given by [30, 31]:

$$\mathrm{IP} = \mathrm{E}^{+} - \mathrm{E}^{0} \tag{1}$$

$$\mathrm{EA} = \mathrm{E}^{0} - \mathrm{E}^{-} \tag{2}$$

where E^{0} ($\mathrm{E}^{\mp}$) is the ground state energy of the neutral (charged) molecule. The HOMO and LUMO, the energy gap ($\mathrm{E_g}$), electronegativity (χ), chemical potential (μ), hardness (η), maximum electronic charge transfer capacity (ΔN_{max}) and softness (S) of the molecules were defined by [32-34]:

$$\chi = \frac{-(\mathrm{E_{LUMO}} + \mathrm{E_{HOMO}})}{2}, \tag{3}$$

$$\mu = -\chi, \tag{4}$$

$$\eta = \frac{(\mathrm{E_{LUMO}} - \mathrm{E_{HOMO}})}{2}, \tag{5}$$

$$\Delta N_{max} = \frac{-\mu}{\eta}, \tag{6}$$

$$\mathrm{S} = \frac{1}{\eta}. \tag{7}$$

It was reported that under the certain conditions, the hardness and softness of a molecule are reliable indicators of the molecular chemical stability, and both are measures of reactivity and resistance to polarization [35]. The half of energy gap represented by the hardness (η), which is associated inversely with the softness (S). whereas the electrochemical reaction is measured by the chemical potential (μ), which is the negative of the electronegativity (χ).

3. Results and Discussions

3.1. Electronic structure and properties of the metal-fullerenes C_{60} complexes

Our aim to investigate the favorable position of metallic atom outside the exohedral doped fullerene C_{60}. These metals include Co, Cu, Fe, Ni, Ru and Pt, which located at three positions outside the cage of C_{60}. The metallic atom could be placed at the centre of diatomic-π bond (C-C), hexagon and pentagon position of fullerene. The structures of all these cases are sufficiently optimized, leading to the metallofullerene molecules shown in Figures (1-3).

Recently, the stable configurations were obtained due to placing metal atom on top of a diatomic-π bond (C-C) position of fullerene C_{60}, whether the (C-C) position is between two hexagons or hexagon and a pentagon [36]. In the present study, we consider the three models of fullerenes-metal complexes, including different positions of the metal atom on the surface of fullerene C_{60}.

3. 1. 1. Frontier molecular orbital

The top panels of Figures (1-3) show different views of the calculated geometries of doped C_{60} fullerene. Whereas the lower panels of Figures (1-3) show the frontier molecular orbitals of all metallofullerene molecules. Red corresponds to the positive and green to the negative regions of the wave function. The calculation shows that the HOMO of C_{60} fullerene with Co, Cu and Fe atoms in the diatomic-π bond position (Figure 1) is delocalized across their surface with significant distribution

around the Cu and Fe atom, while there is scarcity of the HOMO distribution around C_{60} fullerene in the presence of Ni, Pt and Ru atoms. The LUMO is delocalized through the C_{60} with Co, Fe, Ni and Pt atoms, while for the C_{60} with Cu and Ru atoms, the LUMO is almost empty across the C_{60} cage with high distribution around the metals.

Figure 2 (Low panel) shows frontier molecular orbitals for the metallofullerene, where each metallic atoms linked in hexagon position. The HOMO is delocalized across the C_{60} surface and the Co, Cu and Ni atoms have low distribution, while in the presence of Fe, Pt and Ru atoms the HOMO is partially distributed with high frontier orbitals around these metals. Whereas the LUMO is distributed through the C_{60} cage and populated around the Pt and Ru atoms.

For the C_{60} fullerene with metallic atoms linked in pentagon position (see Figure 3), the plots show that the HOMO and LUMO are distributed over the whole molecule for all cases with high distributed of HOMO around Cu atom and high distributed of LUMO around Pt atom.

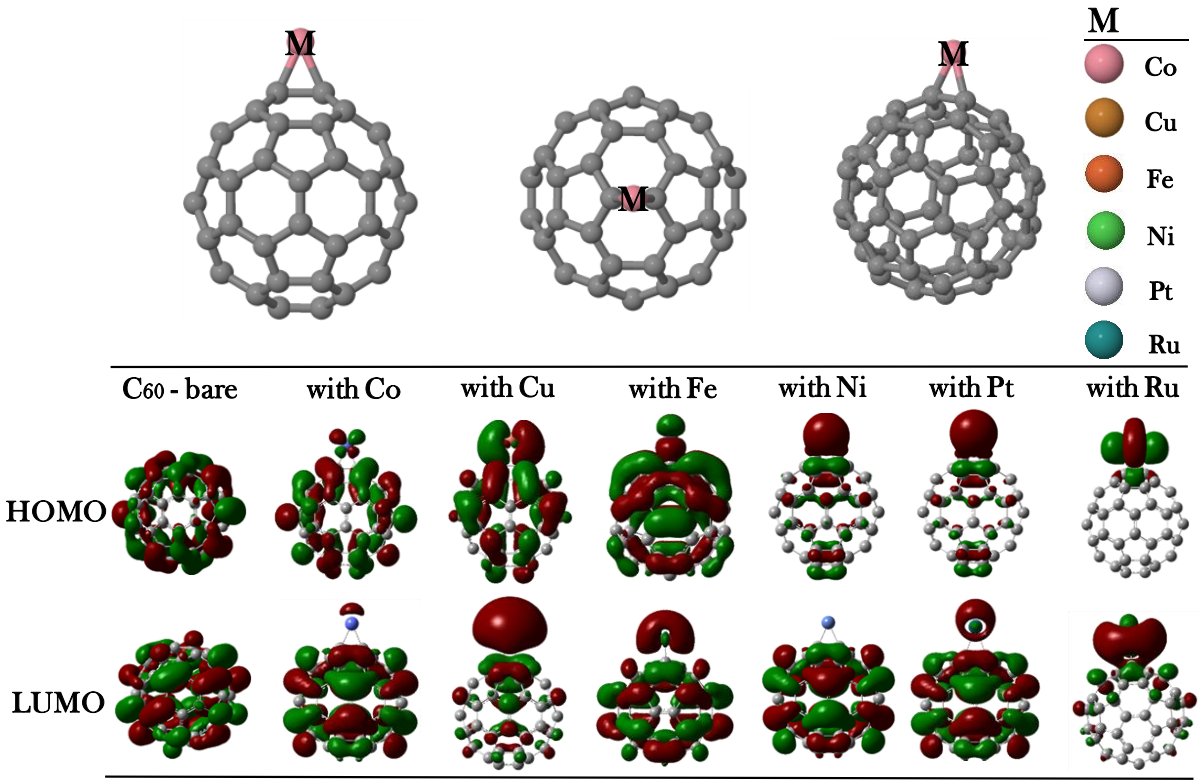

Figure 1. Top panel: An example of different views of the optimised geometry for C_{60} fullerene with different metal atoms (Co, Cu, Fe, Ni, Pt and Ru) linked in diatomic-π bond position. Lower panel: B3LYB-DFT calculation of frontier molecular orbitals (FMOs). Red corresponds to positive and green to negative regions of the wave functions.

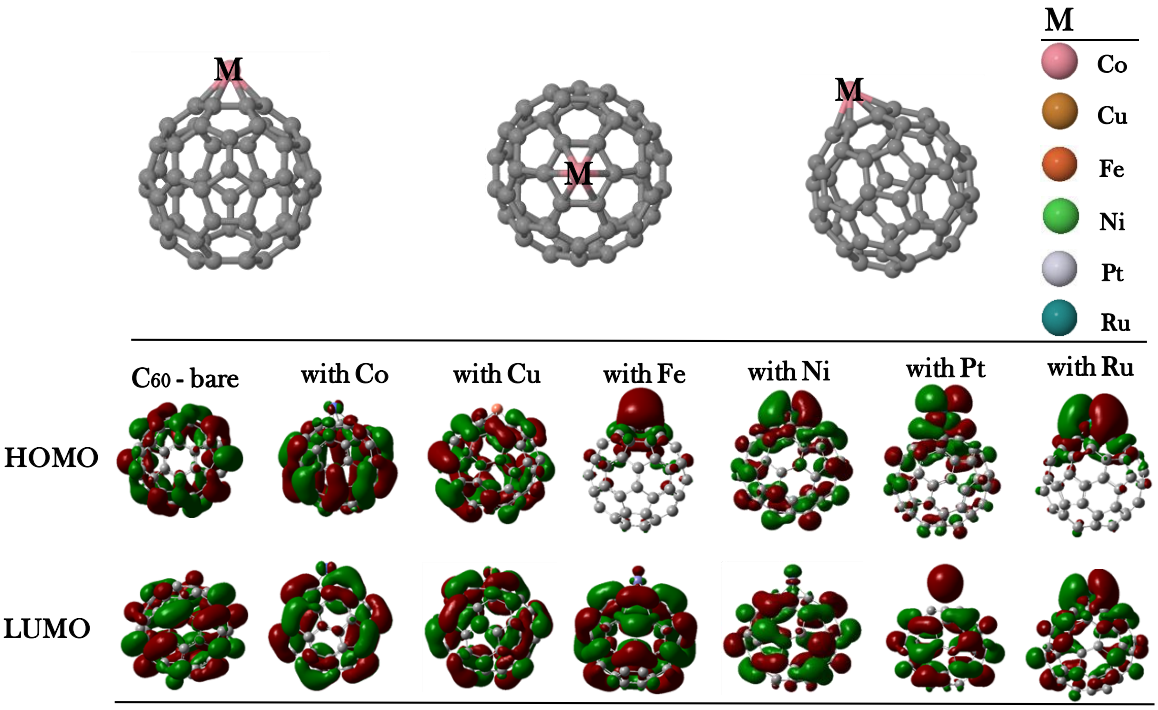

Figure 2. Top panel: An example of different views of the optimised geometry for C_{60} fullerene with different metal atoms (Co, Cu, Fe, Ni, Pt and Ru) linked in hexagon position. Lower panel: B3LYB-DFT calculation of frontier molecular orbitals (FMOs). Red corresponds to positive and green to negative regions of the wave functions.

After obtaining the relaxed geometry of each C_{60} metallofullerene, then the bond lengths between the metal and the centre of diatomic (C-C), hexagon and pentagon were calculated (see Figure 4). The calculation shows that the doped exohedral over the hexagon and pentagon rings are stable in the most states of metal atoms, which agrees well with the previous DFT study [37].

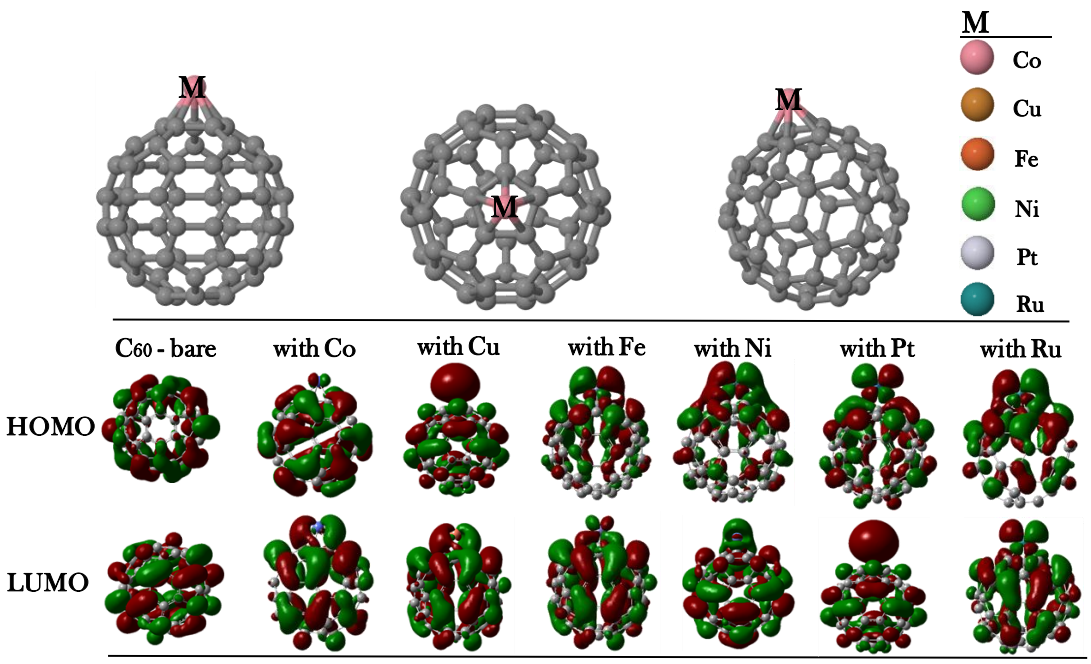

Figure 3. Top panel: An example of different views of the optimised geometry for C_{60} fullerene with different metal atoms (Co, Cu, Fe, Ni, Pt and Ru) linked in pentagon position. Lower panel: B3LYB-DFT calculation of frontier molecular orbitals (FMOs). Red corresponds to positive and green to negative regions of the wave functions.

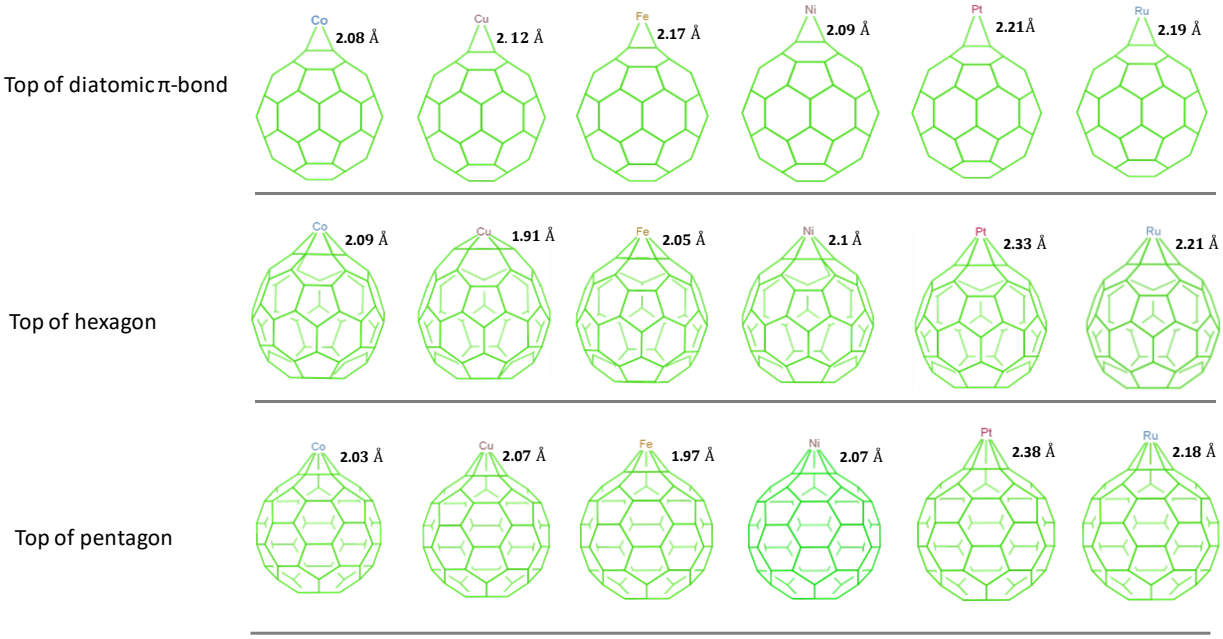

Figure 4. Optimised geometries of the C_{60} exohedral metallofullerenes using the DFT-B3LYP hybrid functionals with **LanL2DZ** basis set for metal atoms **M** and **6-31G(d,p)** for carbon atoms.

3. 1. 2. Electronic properties of exohedral metallofullerene

To explore the qualitative chemical and physical perceptions for each exohedral metallofullerene, the electronic properties were calculated, shown in Tables (1-3). The charge transfer ($+\Delta N$) between the metal atom and the fullerene C_{60} with each of the three different positions (diatomic, hexagon and pentagon position) was computed using B3LYB-DFT.

The calculations show that all metals donate electrons to the fullerene. The resulting ionization potential reveals that the C_{60} fullerene with Co atom linked in the diatomic position has the largest value (IP = 8.4), while the largest electron affinity is found with Fe-hexagon position (EA = 4.7 eV) than those the rest metals. The lowest values of IP and EA are found in the presence of Fe and Co atoms (5.5 and 1.4 eV), respectively.

The larger and smaller energy gaps are obtained for Co-hexagon position (E_g = 2.7 eV) and Cu-hexagon position (E_g = 0.6 eV), respectively. Overall, the calculations suggest that the C_{60} fullerene in the presence of Co often implies a more stability, while C_{60} fullerene with Cu suggests higher reactivity.

Corresponding results for the electronegativities χ are in the range of 5.53 (Ni)-hexagon position to 4.35 (Cu)-diatomic position., whereas the hardness (η) values are in the range of 0.3 (Cu) to 1.34 (Co), where both are found on the hexagon position. The largest softness value is found for Co-hexagon position (S = 3.3), while the smallest value is obtained for Co-hexagon position (S = 0.75). These parameters play role to identify the stable conformation and electronic configuration of a metallofullerene like C_{60}, which depends on the interactions between the metal atom and the fullerene cage.

Determining the electronegativity value of a metal atom bounded on the external surface of the C_{60} fullerene might predict the type of bond is ionic/covalent and the polarity of molecule, which gives insight into how readily the molecule accepts or donates electrons. All the C_{60} fullerene with varied metals have large electronegativity. The Ni atom on the top of hexagon position of C_{60} reveals the larger electronegativity, suggesting an ionic bond between the Ni atom and fullerene cage with fewer polarity than those in the rest metals. However, the properties of interest are represented by determining the charge transfer from the metal to the fullerene, the HOMO/LUMO energy levels

and electron affinity, effecting on the confinement effects, the stability and redox properties of the molecular complex.

Table 1. Calculated charge transfer $+\Delta N$, HOMO, LUMO, ionization potential (IP), electron affinity (EA), energy gap (E_g), electronegativity (χ), chemical potential (μ), global hardness (η), maximum electronic charge transfer capacity (ΔN_{max}) and global softness (S) for C_{60} fullerene with different metal atoms (Co, Cu, Fe, Ni, Pt and Ru) linked in diatomic position.

Metal atoms	$+\Delta N$	HOMO (eV)	LUMO (eV)	IP (eV)	EA (eV)	E_g (eV)	χ	μ	η	ΔN_{max}	S
Bare	0.00	-6.69	-3.87	7.89	2.68	2.82	5.30	-5.30	1.41	3.76	0.71
Co	0.382	-6.28	-3.66	8.40	1.40	2.62	4.97	-4.97	1.31	3.80	0.76
Cu	0.53	-4.84	-3.85	6.00	2.72	0.99	4.35	-4.35	0.50	0.70	2.02
Fe	0.405	-5.99	-3.65	5.50	4.20	2.34	4.82	-4.82	1.17	4.12	0.85
Ni	0.281	-6.13	-3.74	7.10	2.60	2.39	4.94	-4.94	1.19	4.15	0.84
Pt	0.275	-6.28	-3.91	7.61	2.71	2.37	5.10	-5.10	1.2	4.25	0.84
Ru	0.376	-5.47	-3.90	6.21	3.71	1.57	4.69	-4.69	0.78	6.02	1.28

Table 2. Calculated charge transfer $+\Delta N$, HOMO, LUMO, ionization potential (IP), electron affinity (EA), energy gap (E_g), electronegativity (χ), chemical potential (μ), global hardness (η), maximum electronic charge transfer capacity (ΔN_{max}) and global softness (S) for C_{60} fullerene with different metal atoms (Co, Cu, Fe, Ni, Pt and Ru) linked in hexagon position.

Metal atoms	$+\Delta N$	HOMO (eV)	LUMO (eV)	IP (eV)	EA (eV)	E_g (eV)	χ	μ	η	ΔN_{max}	S
Bare	0.00	-6.69	-3.87	7.89	2.68	2.82	5.30	-5.30	1.41	3.76	0.71
Co	0.578	-6.50	-3.82	8.0	1.40	2.70	5.20	-5.20	1.34	3.88	0.75
Cu	0.653	-5.24	-4.63	6.37	3.40	0.62	4.93	-4.93	0.31	15.9	3.30
Fe	0.49	-5.80	-3.82	5.95	4.70	1.98	4.81	-4.81	0.99	4.86	1.01
Ni	0.38	-6.51	-4.55	7.05	3.44	1.95	5.53	-5.53	0.98	5.64	1.03
Pt	0.212	-5.90	-3.99	7.06	2.85	1.90	4.94	-4.94	0.95	5.20	1.05
Ru	0.695	-5.79	-4.43	6.52	4.32	1.35	5.11	-5.11	0.68	7.50	1.48

Table 3. Calculated charge transfer $+\Delta N$, HOMO, LUMO, ionization potential (IP), electron affinity (EA), energy gap (E_g), electronegativity (χ), chemical potential (μ), global hardness (η), maximum electronic charge transfer capacity (ΔN_{max}) and global softness (S) for C_{60} fullerene with different metal atoms (Co, Cu, Fe, Ni, Pt and Ru) linked in pentagon position.

Metal atoms	$+\Delta N$	HOMO (eV)	LUMO (eV)	IP (eV)	EA (eV)	E_g (eV)	χ	μ	η	ΔN_{max}	S
Bare	0.00	-6.69	-3.87	7.89	2.68	2.82	5.30	-5.30	1.41	3.76	0.71
Co	0.588	-6.37	-3.88	7.80	1.75	2.48	5.13	-5.13	1.24	4.14	0.81
Cu	0.47	-4.74	-3.96	5.88	2.80	0.78	4.35	-4.35	0.38	11.45	2.56
Fe	0.38	-5.21	-4.06	5.58	4.30	1.15	4.64	-4.64	0.57	8.14	1.75

Ni	0.346	-5.82	-3.87	6.24	2.71	1.95	4.84	-4.84	0.98	4.94	1.02
Pt	0.342	-6.10	-4.16	7.21	3.06	1.94	5.13	-5.13	0.97	5.30	1.03
Ru	0.61	-5.66	-4.86	6.56	4.05	0.80	5.26	-5.26	0.40	13.15	2.51

3. 1. 3. Density of states (DOS)

To explain the number of available electron states per unit of energy, the density of states (DOS) spectrum calculations were performed for all exodedral metallofulerene molecules, shown in Figure 5*(a)*-*(c)*. The results show that the DOS characterized by peaks and valleys, which refer to energy regions with many and few electron states, respectively. The most intense peaks correspond to the higher density of electron, which appears for C_{60} with Ru on hexagon and pentagon locations around the energy -0.6 eV of the lower unoccupied states, while the valleys, where the lower density of electron appears with Ni-pentagon position.

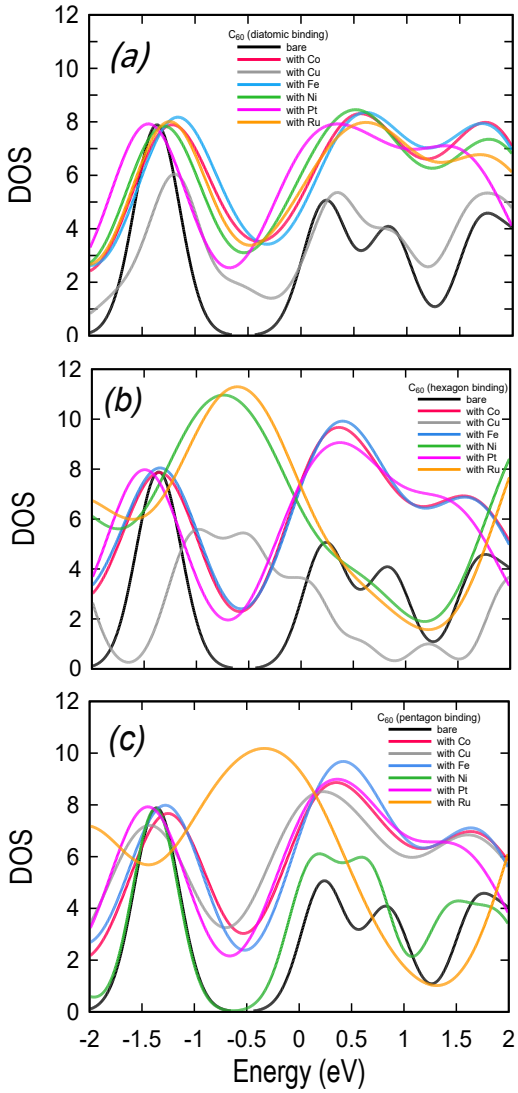

Figure 5. (colour online), *(a)-(c)* B3LYB-DFT calculation of the density of states spectrum (DOS) over a range of energies for C_{60} fullerene with different metal atoms (Co, Cu, Fe, Ni, Pt and Ru) linked in *(a)* diatomic-π bond position, *(b)* hexagon position and *(c)* pentagon position.

The comparison of DOS calculations between the three central positions of varied metals: Diatomic π-bond, hexagon and pentagon of C_{60} fullerene cage. The calculation shows the highest density of electron appears on the energy -0.85 eV of the lower unoccupied states for C_{60} with Ni and Ru on hexagon position, while the DOS spectra shift to the energy 0.35 eV of the high occupied states for C_{60} with Co, Fe and Pt on hexagon position. The pentagon positions reveal high electron states in all transition metals accept with Ni is low. In contrary with the Diatomic positions exhibit low electron states transition metals accept with Ni is high, as shown in Figure 6*(a)-(f)*.

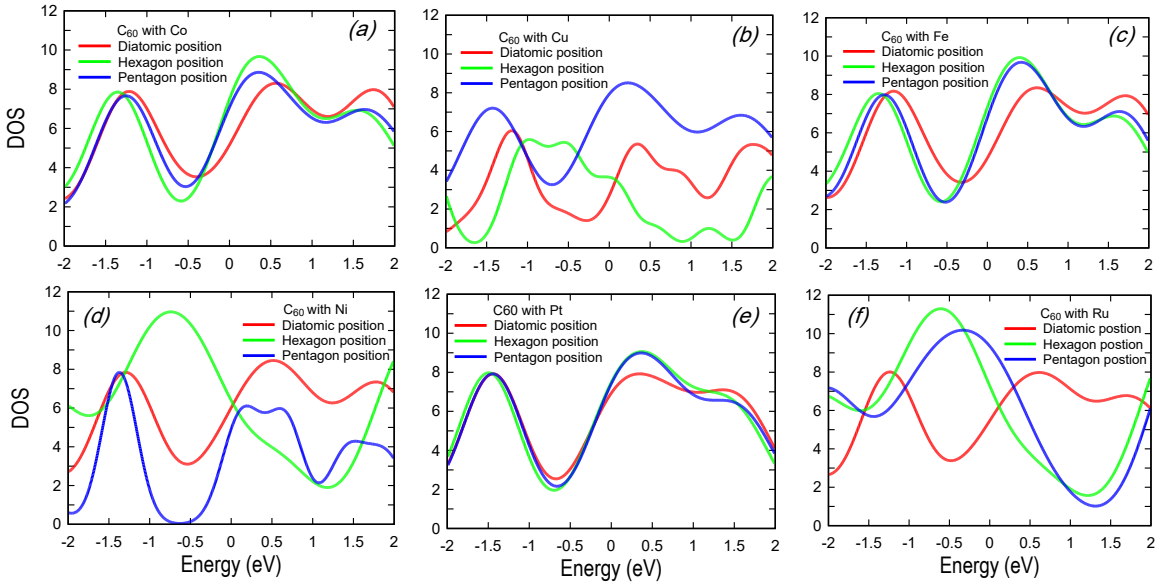

Figure 6. *(a)-(f)* Comparison of DOS calculations between the three different positions: Diatomic π-bond, hexagon and pentagon of C_{60} fullerene with varied metal atoms (Co, Cu, Fe, Ni, Pt and Ru).

3.1.4. Effect on molecular dipole moment

The crucial physical quantity for controlling the self-assembly and tuning both the physical and chemical properties of exohedral metallofullerenes is the dipole moment. Herein, we calculated the dipole moment effect through metallo-fullerene C_{60} with varied metal atoms on the three different locations of outer surface of C_{60} cage, shown in Figure 7. The highest dipole moment was obtained for C_{60} with Cu on the top of diatomic π-bond position, while the lowest was found for Pt on the top of hexagon position. As expected, the calculation shows that the C_{60}-bare (without metal) possesses zero dipole moment, resulting from its high symmetry (non-polar molecule). However, the formed exohedral functionalization breaks this symmetry, leading to produce a dipole moment, which plays role for altering the optical and electronic behaviour of of the C_{60} complexes. The diatomic and pentagon positions of metals almost reveal the higher dipole moment than those in the hexagon position. These confirm that the dipole moment of exohedral metallofullerene depends on the position bond on the outer of surface and the type of metal.

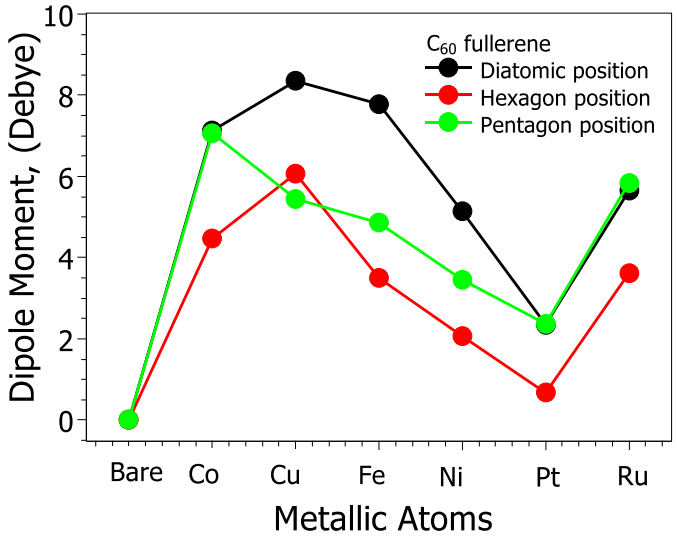

Figure 7. DFT calculation of dipole moment for each Metallo-fullerene C_{60} linked in diatomic position (black), hexagon position (red) and pentagon position (green).

3. 2 Optical properties

3. 2. 1 Ultraviolet spectrum (UV):

For more mapping of electronic structure of the exohedral metallofullerene, we calculated the Ultraviolet spectrum (UV) as a function of wave length using the (TD-DFT)/B3LYP with the basis set of LanL2DZ for metallic atom M and 6-31G(d,p) for carbon atoms. The different UV spectra are associated with the varied metal atoms on the top of central position of three bounded states (diatomic, hexagon and pentagon), shown in Figure 8(*a*)-(*c*) (Left). The UV spectrum results can probe the oxidation state, which helps estimate the charge transferred from the metal atom to the fullerene cage. Moreover, altering UV spectra provide an insight into sensitivity of doping in the fullerene cage. The calculations show that the stronger absorption appears for fullerene with Pt atom in the diatomic π-bond position at the shorter wave length (λ = 800 nm). The high absorption also exhibits with the Cu, Co and Fe atoms on the top of pentagon position at the wave lengths λ =1350, 2500 and 3000 nm, respectively. However, the narrowest energy gap (0.6 eV) for C_{60} with Cu-hexagon position, leading to the higher response of UV absorber at the wave length λ =1400 nm, while the larger energy gap for C_{60} with Co-hexagon exhibits the lowest absorbance of UV at the same wave length. These reveal that the larger electronic transition and stronger interaction between metals and the external surface of fullerene depend on the position and the type of metal atom. In

general, the doped fullerene by the varied metal atoms on the outer surface of fullerene cage shifts the absorption peaks and alters the absorption intensity.

Figure 8(*d*)-(*f*) (Right) shows the calculated energy change via transition metals complexes, linked in diatomic π-bond (C-C), hexagon and pentagon positions. These state that when the metal interacts with fullerene C_{60} cage, the energy gap between the HOMO and LUMO can decrease. The decreasing of energy gap (E_g) range from 2.81 eV for C_{60}-bare to 0.61, 0.78 and 0.98 eV for C_{60} with Cu in hexagon, pentagon and diatomic positions, respectively. The formed complexes through the choice of metal atom results in energy changes, making them more stable and can potentially affect their electronic properties.

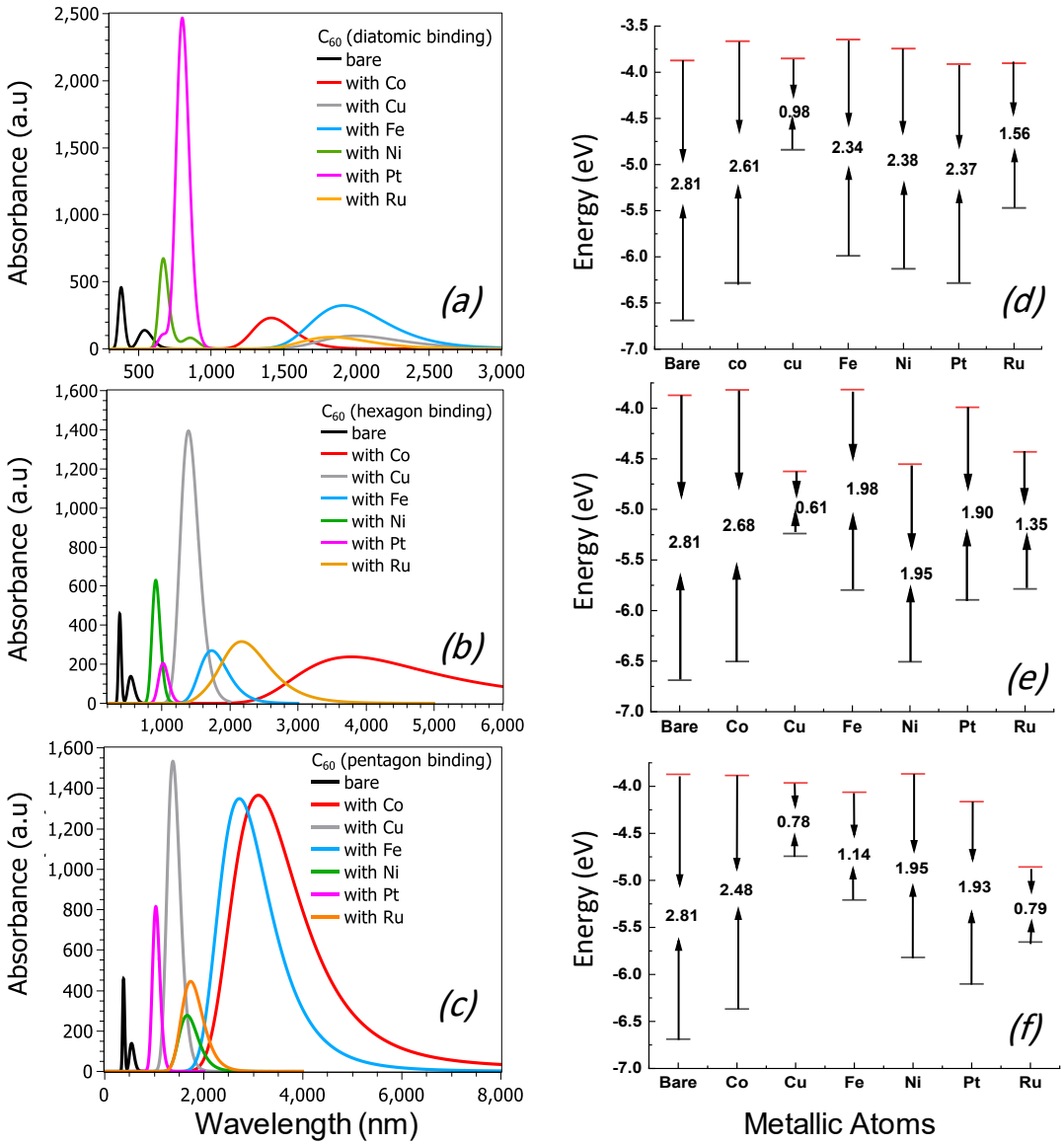

Figure 8. *a-c* (Left) B3LYB-DFT calculation of the UV spectrum over a range of wave lengths for fullerene C_{60} with different metallic atoms (Co, Cu, Fe, Ni, Pt and Ru) linked in *(a)* diatomic-π bond (C-C) position, *(b)* hexagon position and *(c)* pentagon position. The black curve shows the UV spectrum of C_{60} in the bare case. Figures *d-f*. (Right) show the calculation of the energy change upon transition of metals complexes, linked in *(d)* diatomic position, *(e)* hexagon position and *(f)* pentagon position.

Figures 9 (a)-(f) show the comparison of UV spectrum calculation for molecular complexes with each of different three positions (diatomic π bond, hexagon and pentagon). The calculations show that the pentagon position of the C60 with Co, Cu, Fe and Ru reveal the highest absorption at the wavelengths 3200 nm, 1380 nm, 1750 nm, and 1380 nm, respectively. Whereas diatomic position of the C_{60} with Ni and Pt have the higher absorption of UV spectra. These results associated to optimally-bounded metals in three positions on the surface of fullerene cage.

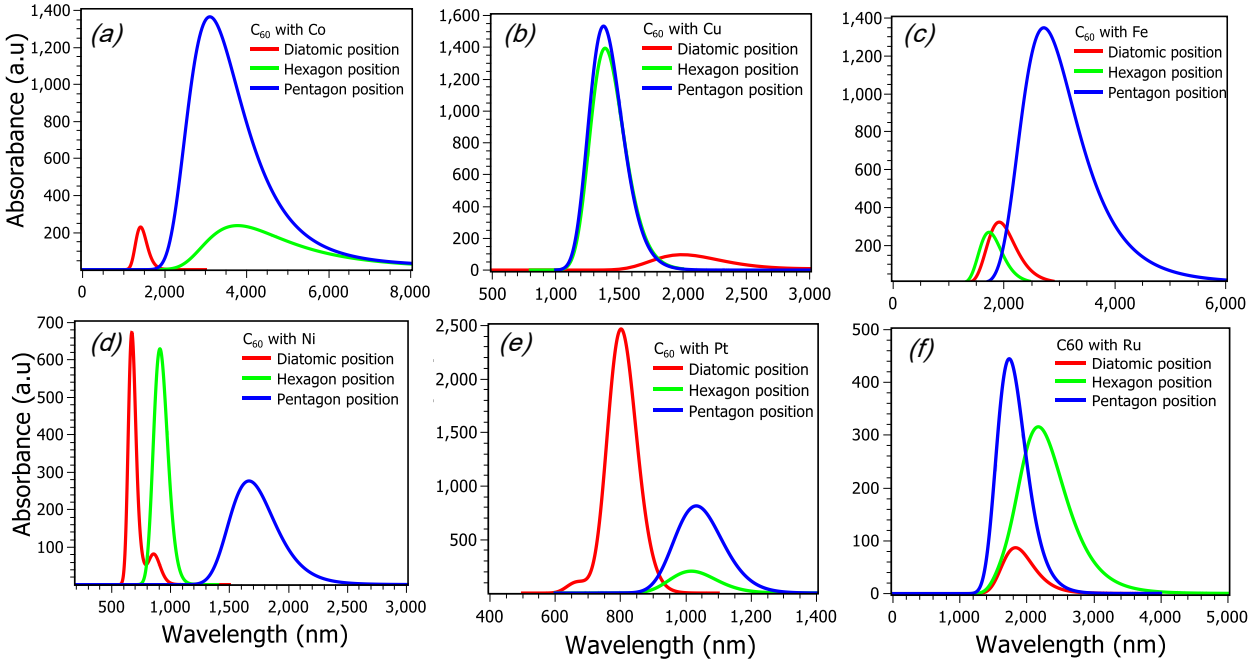

Figure 9. *(a)-(f)* Comparison of UV spectra calculations between the three different positions: Diatomic π-bond, hexagon and pentagon of C_{60} fullerene with varied metal atoms (Co, Cu, Fe, Ni, Pt and Ru).

3. 2. 2. IR spectrum:

To identify the type of bounded metal atom to the fullerene cage, the infrared spectra (IR) of the metallo- fullerene were calculated using TD-DFT/B3LYP with the basis set LanL2DZ, shown in Figures 10-12. The results show that all doped fullerenes with varied metals reveal IR-active modes

due to the asymmetric molecular vibration that absorbs infrared, causing a change in the dipole moment and producing sharp peaks ranged from the wave number 398 cm^{-1} for Cu- pentagon position to 1691 cm^{-1} for Cu- hexagon position. The three positions of Cu atom on the external surface of C_{60} cage exhibit set of vibrational modes, associating with a change in the dipole moment and the highly polarity of the bond. This help to distinguish doping of exohedral fullerene and also probing the structural changes in the fullerene. In general, our calculations show that the doping of metal atom outside the C_{60} fullerene cage significantly changes the vibrational spectrum of exohedral fullerene. The most significant changes in the IR spectra at Cu–carbon cage vibration modes.

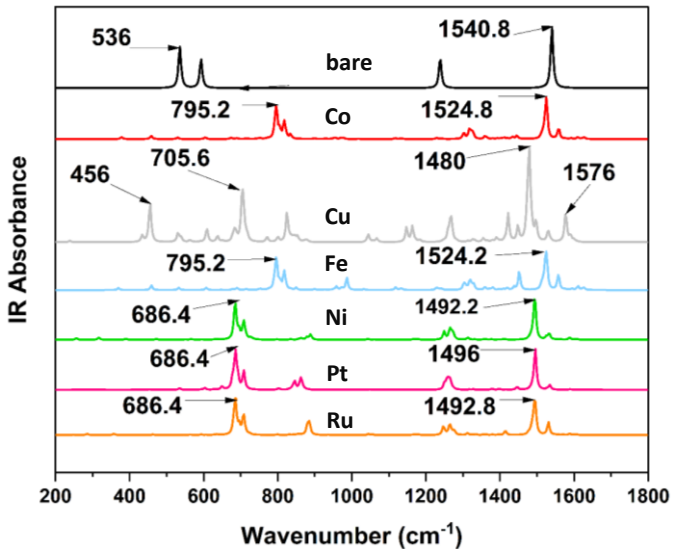

Figure 10. (colour online) The corresponding DFT-calculations of IR spectrum for C_{60} fullerene versus the wave number with different metallic atoms (Co, Cu, Fe, Ni, Pt and Ru), linked in diatomic position.

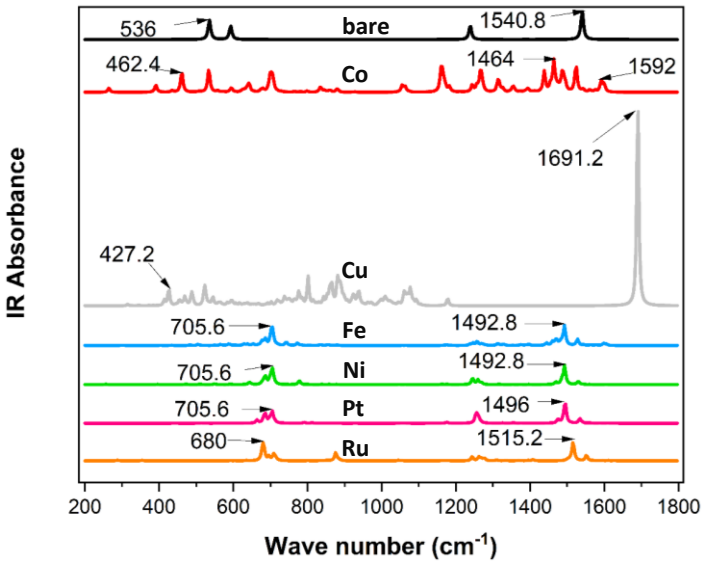

Figure 11. (colour online) The corresponding DFT-calculations of IR spectrum for C_{60} fullerene versus the wave number with different metallic atoms (Co, Cu, Fe, Ni, Pt and Ru), linked in hexagon position.

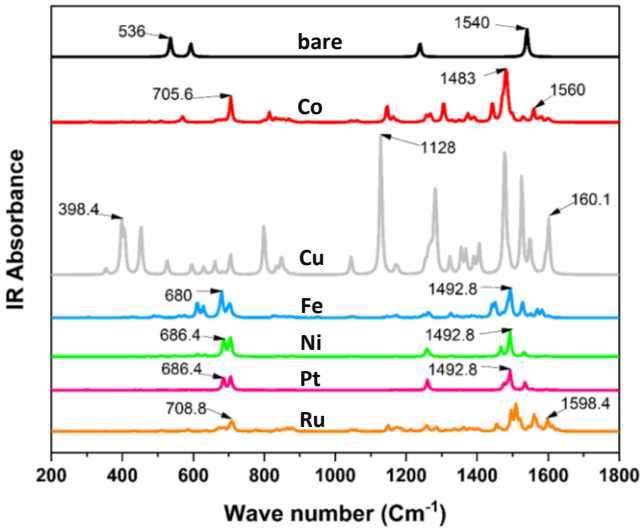

Figure 12. (colour online) The corresponding DFT-calculations of IR spectrum for C_{60} fullerene versus the wave number with different metallic atoms (Co, Cu, Fe, Ni, Pt and Ru), linked in pentagon position.

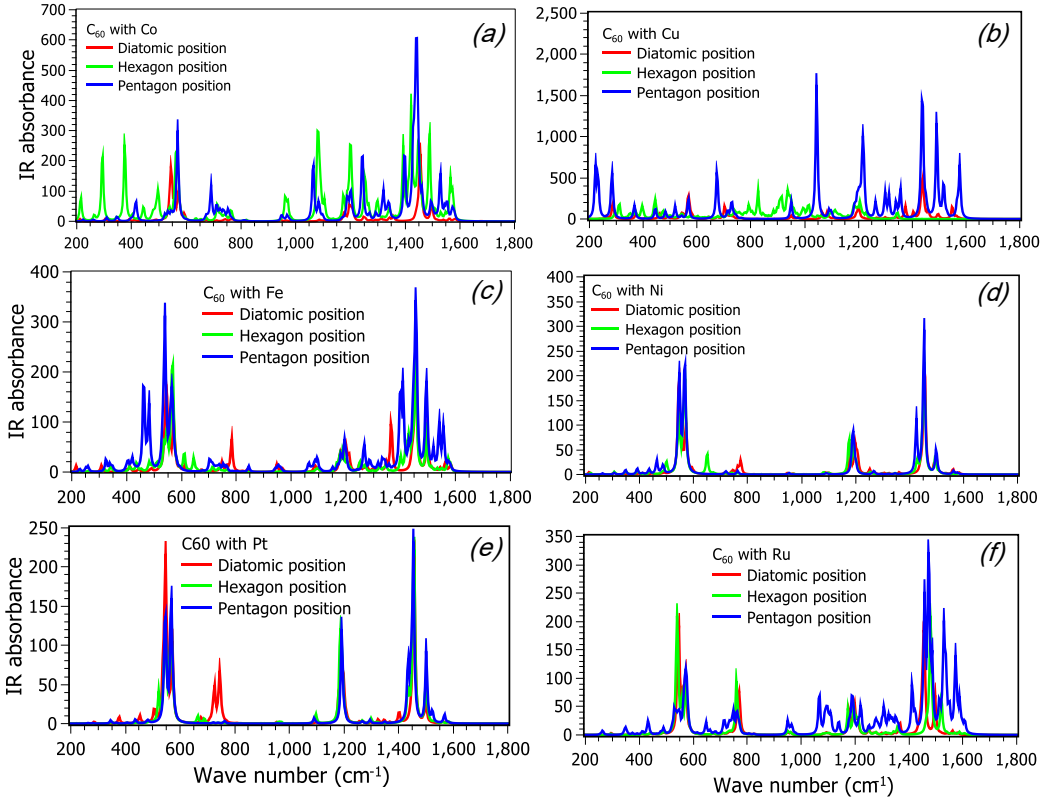

Figure 13. *(a)-(f)* Comparison of IR spectra calculations between the three different positions: Diatomic π-bond, hexagon and pentagon of C_{60} fullerene with varied metal atoms (Co, Cu, Fe, Ni, Pt and Ru).

Figure 13*(a)-(f)* show the comparison of IR spectra calculations due to the binding of each metal on the three positions of fullerene. The stronger absorption of IR is obtained in two locations pentagon and hexagon of fullerene with the six metals.

The comparison calculations of charge transfer, DOS, UV and IR spectrum for three positions suggested that in the most cases the favorite positions of the metal atoms can be found on the pentagon and hexagon of the outer surface of the C_{60}.

4. Conclusions

In summary, we have investigated the electronic and optical properties of exohedral metallofullerene that allows to give rise to complex interaction by varying the metal atoms chosen from the set Co, Cu, Fe, Ni, Pt, and Ru, binding on the top of external surface fullerene cage in three central positions: Diatomic π-bond, hexagon and pentagon. We found that all properties can be tuned with the choice of metal atom and its bond location, leading to support the formation of C_{60} fullerenes hybrids and exhibit their complementary properties. The C_{60} with Cu-hexagon position

has the narrowest energy gap (0.6 eV), resulted to higher response of UV absorber, while the larger energy gap for C_{60} with Co-hexagon exhibits the lowest absorbance of UV at the same wave length. However, the calculations demonstrate the stronger absorption appeared for fullerene with Pt atom in the diatomic π-bond position at the shorter wave length ($\lambda = 800$ nm), which agrees well with previous theoretical investigations [36]. The high absorption also exhibited with the Cu, Co and Fe atoms on the top of pentagon position at the wave lengths λ =1350, 2500 and 3000 nm, respectively. The calculated electronic properties presented insight to discriminate between stable and unstable configurations C_{60} fullerene with varied metals. All of them suggested different responses for the electronic transition, chemical interaction and stable configuration between metals and the external surface of fullerene, which suggested the position and metal-dependent. In general, the doped fullerene by the varied metal atoms on the outer surface of fullerene cage shifts the UV-absorption peaks and alters the absorption intensity with significance changes in the vibrational IR-spectrum of exohedral fullerene. The most significant changes in the IR spectra at Cu–carbon cage vibration modes. The comparison calculations of charge transfer, DOS, UV and IR spectrum suggested that the favorite positions of the metal atoms can be found mostly on the pentagon and hexagon of the outer surface of the C_{60}, which agrees well with the ref. [37]. Our study exhibits the potential of exohedral metallofullerene in future molecular-scale with the multidisciplinary areas, such as electronic and thermoelectric devices.

Declaration of Competing Interest

The authors declare no conflict of interest.

Acknowledgements

The authors acknowledge the Iraqi Ministry of Higher Education and Scientific Research, University of Al-Qadisiyah.

Data Availability Statement

The data that support the findings of this study are available from the corresponding author upon reasonable request.

References:

1. Kroto, H., *The stability of the fullerenes C n, with n= 24, 28, 32, 36, 50, 60 and 70.* Nature, 1987. **329**(6139): p. 529-531.
2. Baskar, A.V., et al., *Self-assembled fullerene nanostructures: synthesis and applications.* Advanced functional materials, 2022. **32**(6): p. 2106924.
3. Chang, X., Y. Xu, and M. von Delius, *Recent advances in supramolecular fullerene chemistry.* Chemical Society Reviews, 2024. **53**(1): p. 47-83.
4. Shen, W., S. Hu, and X. Lu, *Endohedral metallofullerenes: New structures and unseen phenomena.* Chemistry–A European Journal, 2020. **26**(26): p. 5748-5757.
5. Barzaga, R., et al., *On the presence of metallofullerenes in fullerene-rich circumstellar envelopes.* The Astrophysical Journal, 2022. **942**(1): p. 5.
6. Yang, W., et al., *C60 Fullerene-Induced Reduction of Metal Ions: Synthesis of C60-Metal Cluster Heterostructures with High Electrocatalytic Hydrogen-Evolution Performance.* Angewandte Chemie, 2025. **137**(2): p. e202414149.
7. Su, M., et al., *Large-Area Endohedral Metallofullerene Single-Crystal Arrays for High-Performance Field-Effect Transistors and Photodetectors.* Advanced Electronic Materials, 2022. **8**(1): p. 2100753.
8. Bhadra, B.N., et al., *Metal–Organic Framework on Fullerene (MOFOF) as a Hierarchical Composite by the Integration of Coordination Chemistry and Supramolecular Chemistry.* ACS Applied Materials & Interfaces, 2024. **16**(31): p. 41363-41370.
9. Luo, J., et al., *Efficient and stable inverted perovskite solar cells enabled by a fullerene-based hole transport molecule.* Angewandte Chemie International Edition, 2024. **63**(51): p. e202411659.
10. Shen, W., et al., *A Crystalline 2D Fullerene-Based Metal Halide Semiconductor for Efficient and Stable Ideal-bandgap Perovskite Solar Cells.* Advanced Energy Materials, 2024. **14**(23): p. 2400582.
11. Rincón-García, L., et al., *Molecular design and control of fullerene-based bi-thermoelectric materials.* Nature materials, 2016. **15**(3): p. 289-293.
12. Li, W., R. Yang, and M. Sun, *Superior thermoelectric properties of bulk and monolayer fullerene networks.* Journal of Materials Chemistry A, 2023. **11**(8): p. 3949-3960.
13. Wang, R., et al., *Strain engineering of electronic structure and thermoelectric properties of quasi-hexagonal fullerene monolayer.* Journal of Applied Physics, 2024. **136**(1).
14. Ohno, T., et al., *Doping of C60 with iodine.* Nature, 1992. **355**(6359): p. 401-401.
15. Martin, T., et al., *Metal coated fullerene molecules and clusters.* The Journal of chemical physics, 1993. **99**(5): p. 4210-4212.
16. Luo, L., et al., *Nitrogen-Doped Fullerene C60 as High-Performance Anodes for Sodium-Ion Batteries: Enhanced Sodium Adsorption and Storage Capacity.* The Journal of Physical Chemistry Letters, 2025. **16**(7): p. 1753-1759.
17. Saha, S. and S.K. Pati, *Metal-doped fullerene: promising electrocatalysts for hydrogen and oxygen evolution reactions.* Physical Chemistry Chemical Physics, 2025. **27**(22): p. 12024-12031.
18. Robledo, M., et al., *Bonding in exohedral metal–fullerene cationic complexes.* Rsc Advances, 2014. **4**(95): p. 53010-53020.
19. Molina, B., L. Pérez-Manríquez, and R. Salcedo, *Exohedral complexes of large fullerenes, a theoretical approach.* Journal of molecular modeling, 2017. **23**(5): p. 171.
20. Haynes, C.A., S. Lopez, and K.A. Beran, *Investigation into the molecular structure and energetic stability of endohedral and exohedral metallofullerene derivatives of C24.* International Journal of Quantum Chemistry, 2019. **119**(19): p. e25992.
21. Barzaga, R., et al., *Infrared spectral fingerprint of Neutral and Charged Endo-and Exohedral metallofullerenes.* The Astrophysical Journal Supplement Series, 2023. **269**(1): p. 26.

22. Xu, J., et al., *Multifacets of fullerene–metal clusters: From fundamental to application.* Accounts of Chemical Research, 2024. **57**(12): p. 1670-1683.
23. Wang, B., et al., *A Metallofullerene Framework Based on Inherently Chiral Tetranuclear Cuprofullerene Carboxylates.* Crystal Growth & Design, 2024. **24**(16): p. 6566-6571.
24. Garcia-Borràs, M., et al., *Understanding the Exohedral Functionalization of Endohedral Metallofullerenes*, in *Exotic Properties of Carbon Nanomatter: Advances in Physics and Chemistry*. 2015, Springer. p. 67-99.
25. Jin, P., et al., *Exohedral functionalization of endohedral metallofullerenes: Interplay between inside and outside.* Coordination Chemistry Reviews, 2019. **388**: p. 406-439.
26. Moorsom, T., et al., *Reversible spin storage in metal oxide—fullerene heterojunctions.* Science advances, 2020. **6**(12): p. eaax1085.
27. Santha Bhaskaran, A., et al., *Exohedral Diels-Alder Reactivity of Endohedral Metallofullerene C36.* Chemistry–A European Journal, 2024. **30**(58): p. e202401568.
28. Sarfaraz, S., M. Yar, and K. Ayub, *The electronic properties, stability and catalytic activity of metallofullerene (M@ C60) for robust hydrogen evolution reaction: DFT insights.* International Journal of Hydrogen Energy, 2024. **51**: p. 206-221.
29. Frisch, M., et al., *Gaussian 16, revision a. 03, gaussian, inc., wallingford ct.* Gaussian16 (Revision A. 03), 2016.
30. Schildcrout, S.M., R.G. Pearson, and F.E. Stafford, *Ionization potentials of tris (. beta.-diketonate) metal (III) complexes and Koopmans' theorem.* Journal of the American Chemical Society, 1968. **90**(15): p. 4006-4010.
31. Ruoff, R.S., et al., *Relationship between the electron affinities and half-wave reduction potentials of fullerenes, aromatic hydrocarbons, and metal complexes.* The Journal of Physical Chemistry, 1995. **99**(21): p. 8843-8850.
32. Parr, R.G., et al., *Electronegativity: the density functional viewpoint.* The Journal of chemical physics, 1978. **68**(8): p. 3801-3807.
33. Pearson, R.G., *Absolute electronegativity and hardness correlated with molecular orbital theory.* Proceedings of the National Academy of Sciences, 1986. **83**(22): p. 8440-8441.
34. Kar, R., K. Chandrakumar, and S. Pal, *The influence of electric field on the global and local reactivity descriptors: reactivity and stability of weakly bonded complexes.* The Journal of Physical Chemistry A, 2007. **111**(2): p. 375-383.
35. Zaklika, J., et al., *From the electron density gradient to the quantitative reactivity indicators: local softness and the Fukui function.* ACS omega, 2022. **7**(9): p. 7745-7758.
36. Özdamar, B., et al., *Exohedral M–C60 and M2–C60 (M= Pt, Pd) systems as tunable-gap building blocks for nanoarchitecture and nanocatalysis.* The Journal of Chemical Physics, 2015. **143**(11).
37. Sarfaraz, S., et al., *Metallofullerenes as robust single-atom catalysts for adsorption and dissociation of hydrogen molecules: A density functional study.* ACS omega, 2023. **8**(39): p. 36493-36505.